Numerical Simulation of the Flowfield in a Motored Two-Dimensional Wankel Engine

T. I.-P. Shih*
University of Florida, Gainesville, Florida
and
H. J. Schock,† H. L. Nguyen,‡ and J. D. Stegeman‡
NASA Lewis Research Center, Cleveland, Ohio

Numerical solutions were obtained to study the unsteady, multidimensional fluid flow and fuel-air mixing inside the combustion chambers of a motored, two-dimensional Wankel rotary engine during the intake and compression cycles. The effects of the following engine design and operating parameters on fluid flow and fuel-air mixing were investigated: engine speed, direction of gaseous fuel injection into the combustion chamber, and speed of the injected fuel. Results of the numerical study show that engine speed and speed of the injected fuel have significant effects on fluid flow and fuel-air mixing. The direction of fuel injection was found to have less effects on the flow.

Introduction

THE Wankel rotary engine is a promising engine for use in general aviation aircraft.[1-3] Advantages of the Wankel rotary engine over conventional reciprocating piston engines for use in general aviation aircraft include a higher power-to-weight ratio, larger specific power output from higher allowable speed operations, simpler and more compact due to fewer moving parts, and lower noise levels because of less vibration. In addition, the Wankel rotary engine is inherently suited for direct-injection, stratified-charge (DISC) operation. Successful DISC operation will reduce the engine's brake specific fuel consumption by allowing for leaner operations. DISC operation will also reduce pollutant emissions and enhance the engine's multifuel capability.

In order to realize fully these attractive features of the Wankel rotary engine, it is necessary to have a good understanding of how engine design and operating parameters affect the unsteady, multidimensional fluid flow, fuel-air mixing, and combustion inside the engine's combustion chambers. Since the physics taking place inside Wankel engine combustion chambers are exceedingly complex, progress toward understanding the details of these physical processes can be made only in a piecemeal manner by focusing on one aspect of the problem at a time. In addition, it is necessary to make simplifying assumptions. If the assumptions are made judiciously, meaningful results can still be obtained.

To date, only one study has reported details of the unsteady, multidimensional flowfield inside a Wankel rotary engine. Shih et al.[4] reported a numerical study of the flow patterns inside one of the combustion chambers of a motored, two-dimensional Wankel rotary engine with a gaseous fuel injected into the combustion chamber during the compression cycle. In that study, flow patterns inside the combustion chamber during intake, compression, gaseous fuel injection, expansion, and exhaust were calculated for one engine configuration and one engine speed.

So far, no studies have reported the effects of engine design and operating parameters on the details of the fluid flow and fuel-air mixing inside Wankel rotary engines. The objective of this investigation was to numerically study the effects of several engine parameters on fluid flow and fuel-air mixing inside the combustion chambers of a motored, two-dimensional Wankel rotary engine during the intake and compression cycles. The engine parameters studied include: engine speed, direction of gaseous fuel injection, and speed of the injected fuel. A good understanding of how these three engine parameters affect fluid flow and fuel-air mixing is essential for the proper design of DISC Wankel rotary engines.

In the next section, the motored, two-dimensional Wankel rotary engine studied is described. Then, the formulation of the problem, the numerical method of solution, and the results of this numerical study are presented.

Description of the Problem

A schematic diagram of the motored, two-dimensional Wankel rotary engine studied in this investigation is shown in Fig. 1. This engine consists of a shaft, a rotor, a housing, three seals, an intake port, an exhaust port, and three combustion chambers (the three regions bounded by the housing, rotor, and seals). The inner surface of the housing (denoted as surface 1 in Fig. 1) is given by the following parametric equations[4-6]:

$$X_1 = E\cos(3A) + (R+C)\cos(A) \tag{1}$$

$$Y_1 = E\sin(3A) + (R+C)\sin(A) \tag{2}$$

where A is a parametric parameter and it varies between 0 and 2π. E, R, and C are constants given by 0.0154, 0.1064, and 0.004 m, respectively.

The rotor surface (denoted by surfaces 2-4 in Fig. 1) is given by another set of parametric equations involving a parameter V,[4-6]

$$X_2 = E\sin(\theta) + X_{r0}\cos(\theta/3) + Y_{r0}\sin(\theta/3) \tag{3}$$

$$Y_2 = E\cos(\theta) + Y_{r0}\cos(\theta/3) - X_{r0}\sin(\theta/3) \tag{4}$$

Received July 10, 1986; revision received Sept. 12, 1986.

*Assistant Professor, Department of Mechanical Engineering. Member AIAA.
†Deputy Chief, Turbine and Rotary Engine Branch.
‡Aerospace Engineer, Turbine and Rotary Engine Branch.

where

$$\theta = \Omega t \tag{5}$$

$$X_{r0} = X_r \cos(\pi/6) + Y_r \sin(\pi/6) \tag{6}$$

$$Y_{r0} = Y_r \cos(\pi/6) + X_r \sin(\pi/6) \tag{7}$$

$$X_r = R\cos(2V) - (3E^2/R)\sin(6V)\sin(2V) + 2E[1 - (9E^2/R^2)\sin^2(3V)]^{0.5}\cos(3V)\cos(2V) - P_x \tag{8}$$

$$Y_r = R\sin(2V) - (3E^2/R)\sin(6V)\cos(2V) + 2E[1 - (9E^2/R^2)\sin^2(3V)]^{0.5}\cos(3V)\cos(2V) - P_y \tag{9}$$

$$P_x = P\cos(2V) \tag{10}$$

$$P_y = P\sin(2V) \tag{11}$$

Equations (3) and (4) represent surface 2 when V is between $V_L = \pi/6$ and $V_T = \pi/2$, surface 3 when V is between $V_L = 5\pi/6$ and $V_T = 7\pi/6$, and surface 4 when V is between $V_L = 3\pi/2$ and $V_T = 11\pi/6$. Ω, θ, and t in Eq. (5) represent the angular speed of the shaft (also referred to as the engine speed), crankangle, and time, respectively. E, R, and C in Eqs. (8) and (9) have the same values as those used in Eqs. (1) and (2). The P in Eqs. (10) and (11) describes the rotor pocket geometry and is

$$P = 0, \text{ if } V_1 \le V \le V_T \text{ and if } V_L \le V \le V_4$$

$$P = 0.5P_1\{1 - \cos[(V_1 - V)/(V_1 - V_2)]\}, \text{ if } V_2 \le V \le V_1$$

$$P = P_2 + (P_1 - P_2)(V - V_3)/(V_2 - V_3), \text{ if } V_3 \le V \le V_2$$

$$P = 0.5P_2\{1 - \cos[(V - V_4)/(V_3 - V_4)]\}, \text{ if } V_4 \le V \le V_3$$

where

$$P_1 = 0.015 \text{ m}, \quad P_2 = 0.0198 \text{ m}$$

$$V_1 = V_L + 0.875(V_T - V_L)$$

$$V_2 = V_L + 0.75(V_T - V_L)$$

$$V_3 = V_L + 0.4375(V_T - V_L)$$

$$V_4 = V_L + 0.25(V_T - V_L)$$

For this motored, two-dimensional Wankel rotary engine, there is no leakage across the seals. As a result, it is necessary to study only the physical processes taking place inside one of the three combustion chambers. The combustion chamber chosen for study is the region bounded by surfaces 1, 2, 5, and 6 in Fig. 1.

At time t equal to zero, the combustion chamber of interest is located at the beginning of the intake cycle and is filled with air at a uniform temperature of $T_i = 300$ K and a uniform pressure of $P_i = 10^5$ Pa. At this time, the air is in a state of homogeneous turbulence with zero mean velocity. Suddenly, the shaft starts to rotate at a constant angular velocity Ω (Ω equals either 5000 or 10,000 rpm), causing the rotor to rotate in the clockwise direction.

During the intake cycle, air enters the combustion chamber through the intake port. The stagnation temperature and pressure of the air entering through the intake port were maintained at $T_0 = 300$ K and $P_0 = 1.2 \times 10^5$ Pa, respectively. During the early part of the intake cycle, the exhaust port is also open allowing air to leave the combustion chamber. The back pressure of the exhaust port is maintained at $P_b = 0.85 \times 10^5$ Pa. P_b was made less than P_0 to simulate turbocharging conditions.

At crankangle $\theta = 280$ deg, the intake port closes initiating the compression cycle. Between crankangles $\theta_1 = 458$ deg and $\theta_2 = 475$ deg, a gaseous fuel (octane) is injected at an angle α into the combustion chamber (see Fig. 1). α equals one of the following: 30, 45, 60, or 90 deg. The speed V_0 of the gaseous fuel at the fuel injector is given by

$$V_f = V_0(\theta - \theta_1)/3 \text{ deg}, \text{ if } \theta_1 \le \theta \le \theta_1 + 3 \text{ deg}$$

$$= V_0, \text{ if } \theta_1 + 3 \text{ deg} \le \theta \le \theta_2 - 3 \text{ deg}$$

$$= V_0(\theta_2 - \theta)/3 \text{ deg}, \text{ if } \theta_2 - 3 \text{ deg} \le \theta \le \theta_2 \tag{12}$$

In the above equations, $\theta_1 = 458$ deg and $\theta_2 = 475$ deg. V_0 equals either 80 or 160 m/s. The stagnation temperature of the gaseous fuel is maintained at $T_f = 300$ K.

The inner surface of the housing (surface 1 in Fig. 1) and the rotor surface (surface 2) are both maintained at a constant temperature of $T_w = 300$ K. These two surfaces are also impermeable to mass diffusion.

For the problem just described, we are interested in knowing the fluid flow and the mixing of fuel and air during the intake and compression cycles for two different engine speeds (5000 and 10,000 rpm), four different directions of fuel injection (30, 45, 60, and 90 deg), and two different fuel injection speeds (80 and 160 m/s).

Before proceeding with the formulation of this problem, it is noted that the two-dimensional Wankel rotary engine studied in this investigation is more realistic than the one studied in Ref. 4. The rotary engine studied here is different in the following ways: rotor pocket geometry (deep and asymmetric as opposed to shallow and symmetric), stagnation pressure of the intake air (1.2×10^5 Pa as opposed to 1.01×10^5 Pa), back pressure of the exhaust port (0.85×10^5 Pa as opposed to 0.99×10^5 Pa), crankangles during which fuel is injected (between 458 and 475 deg as opposed to between 425 and 487 deg), and speed of the fuel jet as a function of crankangle (an approximate step function as opposed to a sinusoidal function). The Wankel rotary engine studied here closely approximates an experimental Wankel rotary engine from which experimental data for the details of the flowfield will soon be available.

Formulation of the Problem

The equations governing the problem just described are given in Ref. 4 and thus not repeated here. Basically, the governing equations employed were the density-weighted, ensemble-averaged conservation equations of mass, species, x momentum, y momentum, and total energy valid for unsteady, compressible flows of a two-component ideal-gas mixture. The ensemble-averaged conservation equations were

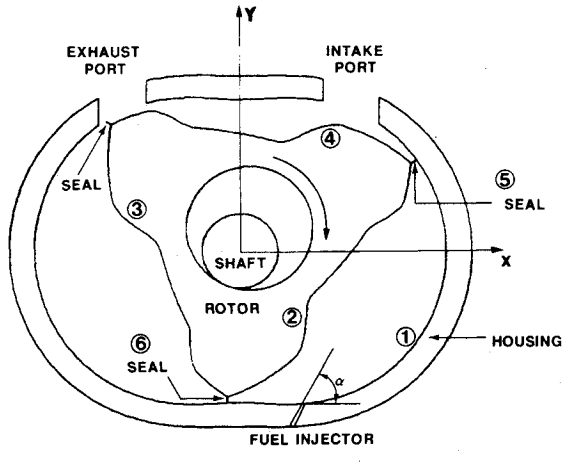

Fig. 1 Schematic diagram of the two-dimensional Wankel rotary engine studied in this investigation.

closed by a variation of the k-ϵ model of turbulence.[7] The particular k-ϵ model employed can account for some of the effects of compressibility,[8] streamline curvature,[9] low Reynolds number effects,[10] and preferential stress dissipation.[11]

The governing equations given in Ref. 4 form a closed system in seven dependent variables: density $\tilde{\rho}$, mass fraction of air $\tilde{X}_A$, x component of the velocity $\tilde{u}$, y component of the velocity $\tilde{v}$, total energy $\tilde{e}$, turbulent kinetic energy K, and dissipation rate of turbulent kinetic energy ϵ. In defining the dependent variables, a tilda over a dependent variable indicates density-weighted ensemble averaging and a bar over a dependent variable indicates unweighted ensemble averaging.

The initial conditions employed were as follows:

$$\tilde{\rho}=P_i M_A/RT_i$$

$$\tilde{X}_A=1,\ \tilde{U}=\tilde{v}=0$$

$$\tilde{e}=P_i[(M_A C_{PA}-R)/R+(h_A^{\circ}-C_{PA}T_i)]$$

$$K \text{ and } \epsilon=\text{const}$$

where M_A is the molecular weight of air, C_{PA} the constant-pressure specific heat of air, h_A° the specific enthalpy of air at T_i, and R the universal gas constant.

The boundary conditions employed at solid walls (i.e., rotor, housing, and seals) were no slip, gas not diffusing into a wall, and gas temperature next to a wall equal to the temperature of the wall. The turbulent kinetic energy and its dissipation rate at the solid walls were set equal to zero because of the turbulence model used.

At the intake port, the boundary conditions employed were as follows. The stagnation temperature and pressure of the intake air were constants. The mass fraction of air was unity. The x component of the velocity was taken to be zero. The y component of the velocity was calculated by the Bernoulli equation, i.e., $\tilde{v}=-C_{DI}[2(P_0-P)/\tilde{\rho}]^{0.5}$, where C_{DI} is the discharge coefficient. The turbulent kinetic energy and its dissipation rate were given by $(n_1\tilde{v})^2$ and $K^{1.5}/(n_2L_1)$, respectively. $n_1=0.03$, $n_2=0.0075$, and L_1 was the length of the intake port.

At the fuel injector, the boundary conditions employed were as follows. The mass fraction of air was zero (since the gas issuing from the fuel injector was octane). The x and y components of the velocity at the fuel injector were $V_0\cos\alpha$ and $V_0\sin\alpha$, respectively. V_0 is given by Eq. (12). The stagnation temperature of the fuel issuing from the fuel injector was kept constant at T_f. The pressure gradient normal to the fuel injector was set to zero. The turbulent kinetic energy and its dissipation rate were calculated by $(n_3\tilde{v})^2$ and $K^{1.5}/(n_3L_2)$, respectively. $n_3=0.03$, $n_4=0.0075$, and L_2 was the length of the fuel injector port.

Numerical Method of Solution

Solutions to the governing equations and the initial and boundary conditions described in the previous section can be obtained only by numerical methods. In this investigation, solutions were obtained by an implicit finite-difference method. In the following, we first discuss the time levels and the grid points at which solutions were obtained. Afterward, we discuss the finite-difference method of solution.

Time Levels and Grid Points

In order to obtain solutions by finite-difference methods (FDM), it is necessary to replace the duration of interest by time levels and the spatial domain of interest by a system of grid points. FDM's give solutions only at the time levels and grid points.

For the present problem, the duration of interest is that of the intake and compression cycles. That continuous period of time must be replaced by a finite number of time levels.

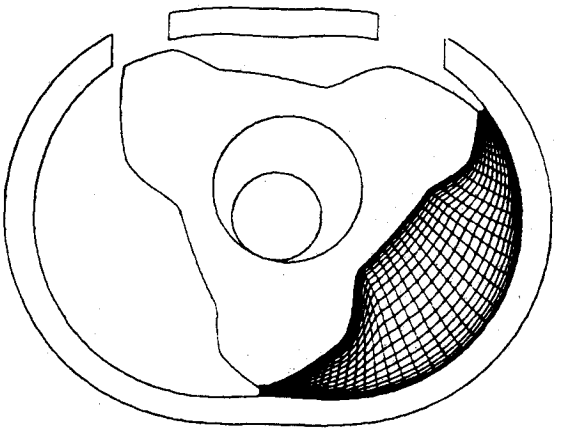

Fig. 2 Grid system in the X-Y-t coordinate system.

The time increment between two successive time levels (known as the time-step size) must be made small enough to ensure numerical stability and temporal accuracy. In this study, variable time-step sizes were used. Very small time-step sizes were used near the beginning of the intake cycle where the rotor was impulsively started from 0 rpm to either 5000 or 10,000 rpm and where the intake and exhaust ports were suddenly opened, exposing the air inside the combustion chamber to very large pressure gradients. As time progressed, the time-step size was allowed to increase steadily until it reached a prescribed maximum time-step size, $\Delta t_{\max}$. Just before gaseous fuel injection, the time-step size was again reduced. Throughout the gaseous fuel injection, the time-step size used was half of $\Delta t_{\max}$.

The time-step size used between time level n and $n+1$ (denoted by Δt^{n+1}) is given by

$$\Delta t^{n+1}=[\theta(n+1)-\theta(n)]/\Omega \qquad n=1,2,\ldots,n_s$$

$$\Delta t^{n+1}=\Delta\theta_f/\Omega \qquad n=n_s+1,\ldots,n_f$$

$$\Delta t^{n+1}=0.5\Delta\theta_f/\Omega \qquad n=n_f+1,\ldots,n_t$$

where

$$\theta(n)=a_1(n/n_s)+a_2(n/n_s)^2+a_3(n/n_s)^3$$

$$a_3=\frac{1.001\Delta\theta_f-2/n_s}{1/n_s+3/n_s^2+2/n_s^3}$$

$$a_2=\frac{0.001\Delta\theta_f-1/n_s-a_3(1/n_s^3-1/n_s)}{1/n_s^2-1/n_s}$$

$$a_1=1-a_2-a_3$$

$$\Delta\theta_f=(3\pi-1)/(n_t-n_s)$$

$$n_s=800$$

In the above equations, $n_t=5000$ and $n_f=4400$ when $\Omega=5000$ rpm. When $\Omega=10{,}000$ rpm, $n_t=3000$ and $n_f=2600$.

For the present problem, the spatial domain of interest is the combustion chamber bounded by surfaces 1, 2, 5, and 6 in Fig. 1. This continuous domain must be replaced by a system of grid points. For computational efficiency, the number of grid points used should be kept to the minimum that is required to spatially resolve all significant features of the flow. The grid system employed in this study was as follows. In the X-Y-t coordinate system (see Fig. 2), the grid points moved with the combustion chamber; the grid points were not uniformly distributed, with more grid points placed near solid surfaces (rotor, housing, and seals) than elsewhere

to resolve the steep gradients of the dependent variables there; and grid lines intersected the rotor and housing surfaces perpendicularly so that derivative boundary conditions could be implemented accurately. The total number of grid points employed for all of the computations was 1275 (with 25 grid lines from rotor to housing and 51 grid lines from seal to seal).

To facilitate the finite-difference method of solution, the moving and nonuniformly distributed system of grid points in the X-Y-t coordinate system was mapped onto the ξ-η-τ coordinate system. In the ξ-η-τ coordinate system, all of the grid points were stationary and uniformly distributed. This mapping of grid points is known as grid generation. In this study, an algebraic grid generation technique based on transfinite interpolation was employed.[12,13] The functional relationship between the coordinate systems obtained by the grid generation technique employed here is summarized in the Appendix. The detail of the grid generation technique employed is given in Ref. 13.

Finite-Difference Method

In this study, solutions to the governing equations were obtained by the implicit-factored method of Beam and Warming. The implicit-factored method of Beam and Warming is a highly efficient method for obtaining solutions to steady as well as unsteady multidimensional fluid flow problems. The readers are referred to Ref. 14 for the details of the implicit-factored method and to Ref. 15 for the details of implicit implementation of boundary conditions.

Results

Numerical solutions were obtained to study how engine speed, angle of gaseous fuel injection, and speed of the fuel leaving fuel injector affect fluid flow and fuel-air mixing inside one of the combustion chambers of a motored, two-dimensional Wankel rotary engine during the intake and compression cycles. The ranges of the engine parameters studied were as follows: two engine speeds ($\Omega = 5000$ and 10,000 rpm), four different fuel injection angles ($\alpha = 30$, 45, 60, and 90 deg), and two different speeds of the fuel at the fuel injector ($V_0 = 80$ and 160 m/s).

In the following, we first examine the effects of engine speed on fluid flow during the intake cycle and the early part of the compression cycle before gaseous fuel injection. We then examine the effects of engine speed and the angle and speed of fuel injection on fluid flow and fuel-air mixing during the later part of the compression cycle in which fuel was injected.

Intake and Compression Cycles: No Fuel Injection

Fluid flow during the intake cycle and the early part of the compression cycle is shown in Figs. 3–6. It can readily be seen from these figures that fluid flow is strongly affected by engine speed.

One important effect of engine speed on fluid flow can be seen from Figs. 3a and 4a. From these two figures, we note that for the same turbocharging pressures (recall that the stagnation pressure of the intake air is maintained at 1.2×10^5 Pa and the back pressure of the exhaust port is maintained at 0.85×10^5 Pa), the intake air may or may not exit through the exhaust port, depending upon the engine speed. At low engine speeds, the intake air will exit through the exhaust port (Fig. 3a). However, as the engine speed increases, two factors oppose the intake air from exiting the exhaust port. The first factor is time. As engine speed increases, the port overlap time decreases. The second factor is the momentum induced by the rotor. As engine speed increases, the momentum induced by the rotor increases and that momentum will oppose the intake air from leaving through the exhaust port.

Another important effect of engine speed on fluid flow can be seen in Figs. 3–6. At low engine speeds, a large recirculating flow develops on the right side of the intake jet, which persists throughout the intake cycle and part of the compression cycle (Figs. 3 and 5). At high engine speeds, no recirculating flows can be seen on the right side of the intake jet (Figs. 4 and 6). One reason for this might be that, as engine speed increases, the momentum induced by the rotor causes the intake jet to bend toward the right. As the intake jet bends toward the right, the region between the right side of the jet and the housing reduces in size so that the recirculating flow steadily decreases in size until it cannot be simulated on a coarse grid.

Compression Cycle: With Fuel Injection

Figures 7–11 show fluid flow and fuel-air mixing during gaseous fuel injection. Comparisons of Fig. 7 with Fig. 9 and Fig. 8 with Fig. 10 show that the gaseous fuel jet penetrates less and less deeply into the combustion chamber as the engine speed increases. There are two reasons for this: 1) as engine speed increases, the momentum induced by the rotor increases forcing the fuel jet to bend toward the housing; and 2) as engine speed increases, the duration of fuel injection decreases.

Comparisons of Fig. 7 with Fig. 8 and Fig. 9 with Fig. 10 show how the speed of the fuel leaving the fuel injector affects fluid flow. From these figures, it can readily be seen that as the speed of the fuel increases, the gaseous fuel jet penetrates deeper.

From Figs. 7–10, it can be seen that, in all cases, the gaseous fuel jet does not penetrate very deeply into the com-

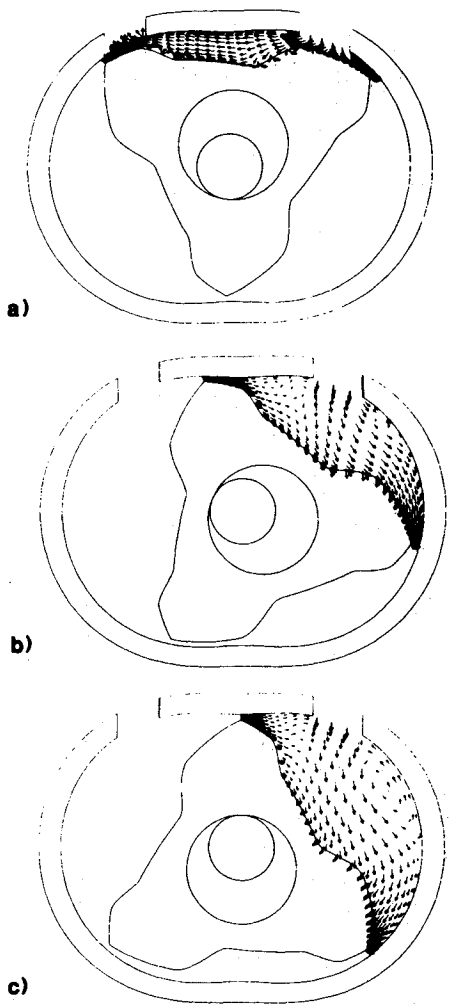

Fig. 3 Fluid flow during the intake cycle at $\Omega = 5000$ rpm: a) $\theta = 10$ deg; b) $\theta = 113$ deg; c) $\theta = 180$ deg.

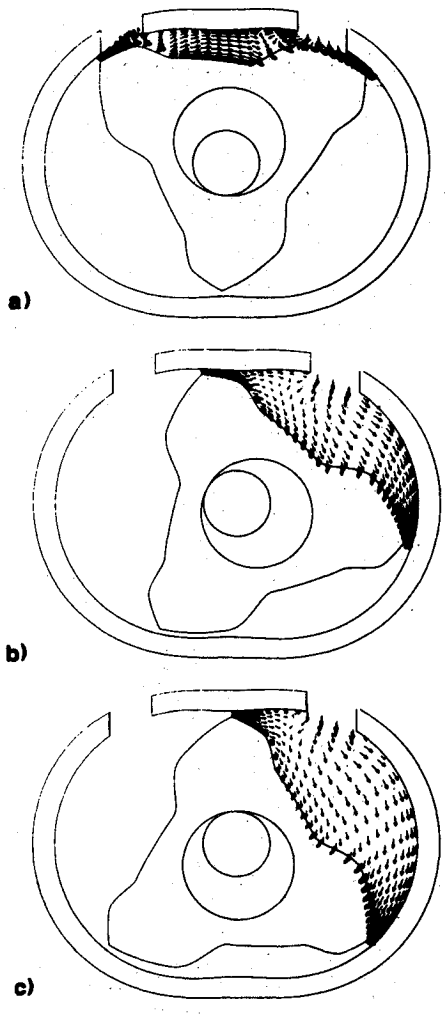

Fig. 4 Fluid flow during the intake cycle at $\Omega = 10{,}000$ rpm: a) $\theta = 9$ deg; b) $\theta = 116$ deg; c) $\theta = 175$ deg.

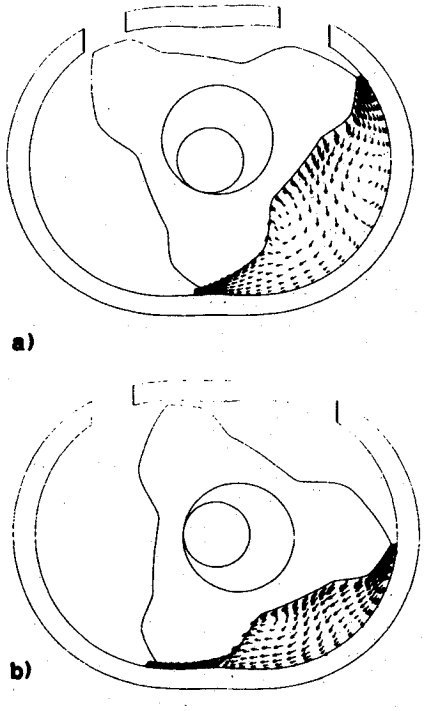

Fig. 5 Fluid flow during the compression cycle before fuel injection at $\Omega = 5000$ rpm: a) $\theta = 380$ deg; b) $\theta = 457$ deg.

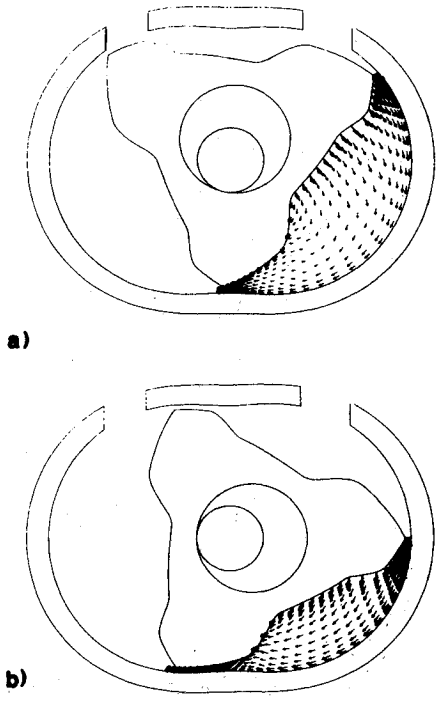

Fig. 6 Fluid flow during the compression cycle before fuel injection at $\Omega = 10{,}000$ rpm: a) $\theta = 371$ deg; b) $\theta = 451$ deg.

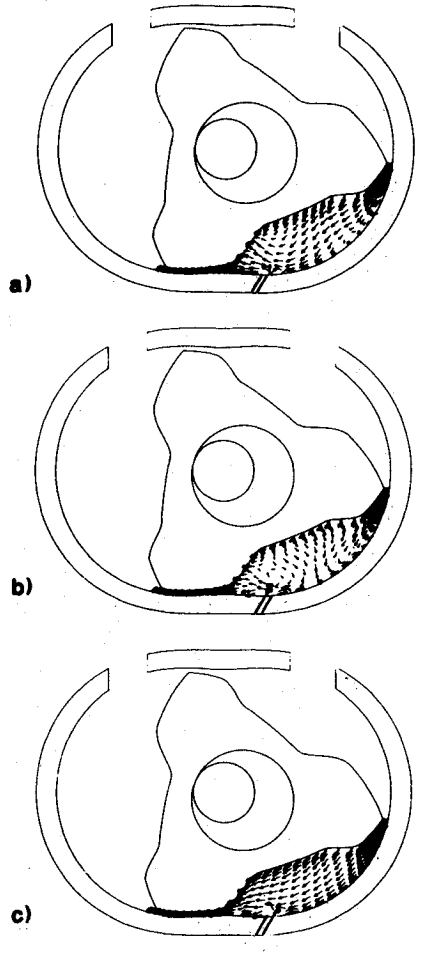

Fig. 7 Fluid flow during fuel injection at $\Omega = 5000$ rpm, $\alpha = 45$ deg, and $V_0 = 80$ m/s: a) $\theta = 461$ deg; b) $\theta = 465$ deg; c) $\theta = 473$ deg.

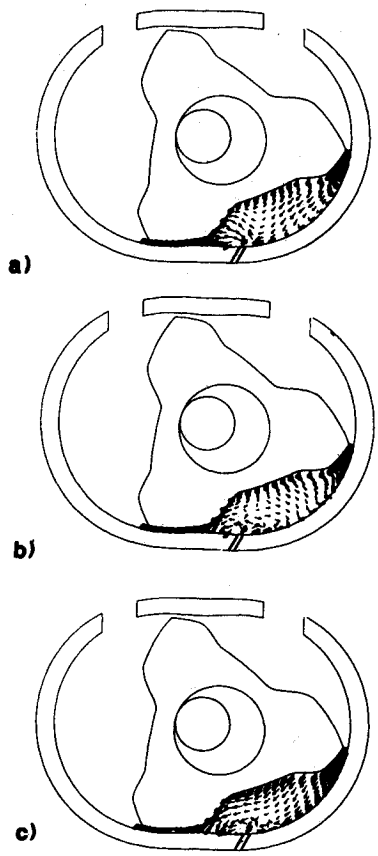

Fig. 8 Fluid flow during fuel injection at $\Omega = 5000$ rpm, $\alpha = 45$ deg, and $V_0 = 160$ m/s: a) $\theta = 461$ deg; b) $\theta = 465$ deg; c) $\theta = 473$ deg.

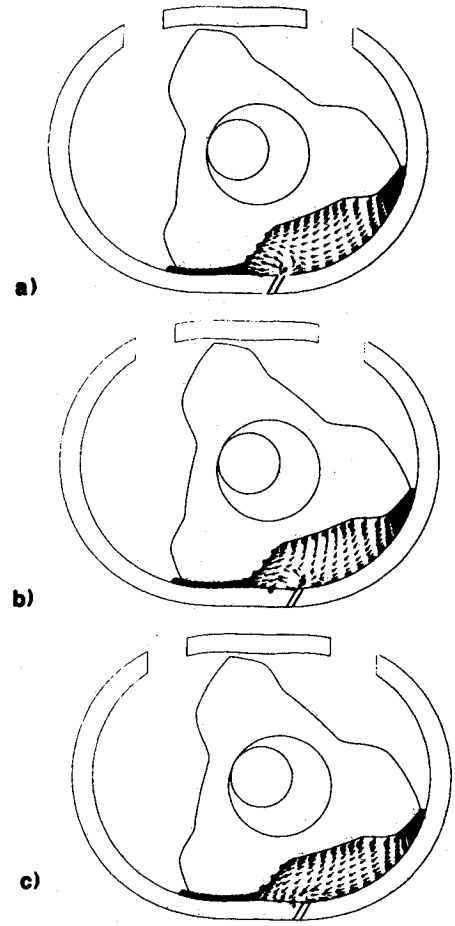

Fig. 10 Fluid flow during fuel injection at $\Omega = 10{,}000$ rpm, $\alpha = 45$ deg, and $V_0 = 160$ m/s: a) $\theta = 462$ deg; b) $\theta = 469$ deg; c) $\theta = 476$ deg.

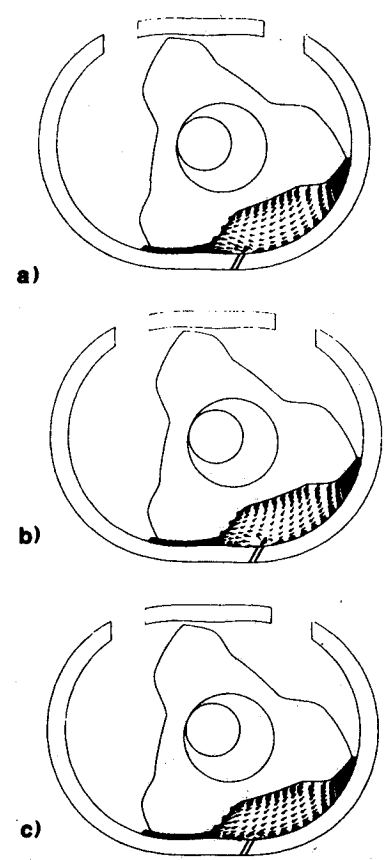

Fig. 9 Fluid flow during fuel injection at $\Omega = 10{,}000$ rpm, $\alpha = 45$ deg, and $V_0 = 80$ m/s: a) $\theta = 461$ deg; b) $\theta = 469$ deg; c) $\theta = 476$ deg.

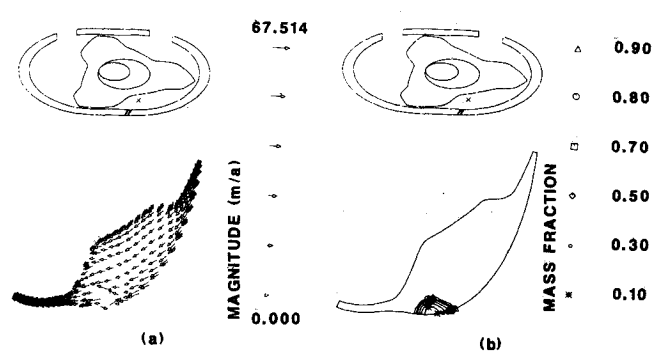

Fig. 11 Fluid flow during fuel injection a) and contour of the mass fraction of air b) at $\Omega = 5000$ rpm, $\alpha = 45$ deg, $V_0 = 80$ m/s, and $\theta = 468$ deg.

bustion chamber. This indicates poor fuel-air mixing, as can be seen in Fig. 11. The depth of penetration shown in Fig. 11 is representative of all the solutions obtained in this study. There are two reasons for the poor penetration of the fuel jet: 1) this is a two-dimensional Wankel rotary engine and the fuel jet is a planar jet in a crossflow (a planar jet can be deflected much more easily than can a three-dimensional jet) and 2) the jet is a gaseous jet instead of a liquid jet (a gaseous jet has much less momentum than a liquid jet).

Results for different angles of fuel injection are not shown because they are similar to those shown in Figs. 7–11. For the two-dimensional Wankel rotary engine studied here, injecting the fuel into the combustion chamber at different angles did not increase penetration nor improve fuel-air mixing.

Here, it is noted that in Ref. 4, the fuel jet did penetrate deeply into the combustion chamber. However, the two-dimensional Wankel rotary engine studied in that reference had a different rotor pocket geometry. Furthermore, in that study, the fuel was injected over a much wider crankangle range of 424–487 deg.

The results obtained here were not compared with experimental data because they do not yet exist.

Conclusions

In this investigation, a numerical study was performed to investigate how engine speed and the angle and speed of gaseous fuel injection affect fluid flow and fuel-air mixing inside a motored, two-dimensional Wankel rotary engine. Engine speed was found to have significant effects on fluid flow. The speed of the fuel jet was also found to have an important effect on fluid flow. From this study, it can be seen that the effects of fuel injection angle on fluid flow in an actual Wankel rotary engine cannot be studied by a two-dimensional simulation.

Efforts are underway to perform a three-dimensional numerical study of the flowfield inside Wankel rotary engines. A three-dimensional numerical study would be able to account for the physics of jets in cross flows (taking place during intake and fuel injection) and Taylor vortices that may be as large as the size of the combustion chamber.

Appendix

The functional relationship between the X-Y-t coordinate system and the ξ-η-τ coordinate system obtained by the grid generation technique presented in Ref. 13 is given below.

$$X(\xi,\eta,\tau)=X_2(\xi,\tau)h_1(\eta')+X_1(\xi,\tau)h_2(\eta') - K_2(\xi)\frac{\partial Y_2(\xi,\tau)}{\partial\xi}h_3(\eta')-K_1(\xi)\frac{\partial Y_1(\xi,\tau)}{\partial\xi}h_4(\eta') \quad \text{(A1)}$$

$$Y(\xi,\eta,\tau)=Y_2(\xi,\tau)h_1(\eta')+Y_1(\xi,\tau)h_2(\eta') + K_2(\xi)\frac{\partial X_2(\xi,\tau)}{\partial\xi}h_3(\eta')+K_1(\xi)\frac{\partial X_1(\xi,\tau)}{\partial\xi}h_4(\eta') \quad \text{(A2)}$$

$$t=\tau \quad \text{(A3)}$$

where

$$h_1(\eta')=2(\eta')^3-3(\eta')^2+1 \quad \text{(A4)}$$

$$h_2(\eta')=-2(\eta')^3+3(\eta')^2 \quad \text{(A5)}$$

$$h_3(\eta')=(\eta')^3-2(\eta')^2+\eta' \quad \text{(A6)}$$

$$h_4(\eta')=(\eta')^3-(\eta')^2 \quad \text{(A7)}$$

$$\eta'=0.5(B_\eta+1)-B_\eta\left[1+\left(\frac{B_\eta+1}{B_\eta-1}\right)^{(2\eta-1)}\right]^{-1} \quad \text{(A8)}$$

$$1-\frac{A-A_L}{A_T-A_L}=0.5(B_\xi+1) - B_\xi\left[1+\left(\frac{B_\xi+1}{B_\xi-1}\right)^{(2\xi-1)}\right]^{-1} \quad \text{(A9)}$$

$$1-\frac{V-V_L}{V_T-V_L}=0.5(B_\xi+1) - B_\xi\left[1+\left(\frac{B_\xi+1}{B_\xi-1}\right)^{(2\xi-1)}\right]^{-1} \quad \text{(A10)}$$

$$K_1(\xi)=K_2(\xi)=2\{[X_1(\xi,\tau)-X_2(\xi,\tau)]^2 + [Y_1(\xi,\tau)-Y_2(\xi,\tau)]^2\}^{1/2} \quad \text{(A11)}$$

$$B_\xi=(1-B_1)^{-0.5} \quad \text{(A12)}$$

$$B_\eta=(1-B_2)^{-0.5} \quad \text{(A13)}$$

In the above equations, X_1, Y_1, X_2, and Y_2 are given by Eqs. (1-11). The parameter A in Eqs. (1) and (2) is related to ξ by Eq. (A9) and the parameter V in Eqs. (8-11) is related to ξ by Eq. (A10). B_1 and B_2 are equal to 0.1 and 0.2, respectively.

The metric coefficients needed to obtain solutions to the governing equations are evaluated from

$$\xi_x=\frac{\partial\xi}{\partial X}=JY_\eta \quad \text{(A14)}$$

$$\xi_y=\frac{\partial\xi}{\partial Y}=-JX_\eta \quad \text{(A15)}$$

$$\xi_t=\frac{\partial\xi}{\partial t}=J(Y_\tau X_\eta-X_\tau Y_\eta) \quad \text{(A16)}$$

$$\eta_x=\frac{\partial\eta}{\partial X}=-JY_\xi \quad \text{(A17)}$$

$$\eta_y=\frac{\partial\eta}{\partial Y}=JX_\xi \quad \text{(A18)}$$

$$\eta_t=J(X_\tau Y_\xi-Y_\tau X_\xi) \quad \text{(A19)}$$

$$J=1/(X_\xi Y_\eta-X_\eta Y_\xi) \quad \text{(A20)}$$

with $X_\xi=\partial X/\partial\xi$, $X_\eta=\partial X/\partial\eta$, $X_\tau=\partial X/\partial\tau$, $Y_\xi=\partial Y/\partial\xi$, $Y_\eta=\partial Y/\partial\eta$, and $Y_\tau=\partial Y/\partial\tau$ evaluated numerically instead of analytically to avoid geometrically induced errors.

Acknowledgment

This research was supported by NASA Grant NAG 3-363. The authors are grateful to NASA Lewis Research Center for this support.

References

[1]Willis, E. A. and Strack, W. C., "An Overview of General Aviation Propulsion Research Programs at NASA-Lewis Research Center," SAE Paper 810624, 1981.

[2]Willis, E. A., "Development Potential of Intermittent Combustion (IC) Aircraft Engines for Commuter Transport Applications," SAE Paper 820718, 1982.

[3]Willis, E. A. and Wintucky, W. T., "An Overview of NASA Intermittent Combustion Engine Research," AIAA Paper 84-1393, 1984.

[4]Shih, T. I-P., Yang, S.-L., and Schock, H. J., "A Two-Dimensional Numerical Study of the Flow Inside the Combustion Chambers of a Motored Rotary Engine," SAE Paper 860615, 1986.

[5]Ansdale, R. F., *The Wankel RC Engine—Design and Performance,* Iliffe Books, London, 1968, pp. 131-139.

[6]Yamamoto, K., *Rotary Engine,* Sankaido Co., Tokyo, 1981, pp. 11-13.

[7]Shih, T. I-P., "Mathematical Models for the Numerical Study of Turbulent Flows," Dept. of Mechanical Engineering, University of Florida, Gainesville, CFDL Rept. 8503, Sept. 1985.

[8]Morel, T. and Mansour, N. N., "Modelling of Turbulence in Internal Combustion Engines," SAE Paper 820040, 1982.

[9]Leschziner, M. A. and Rodi, W., "Calculation of Annular and Twin Parallel Jets Using Various Discretization Schemes and Turbulence-Model Variations," *Transactions of ASME, Journal of Fluids Engineering,* Vol. 103, 1981, pp. 352-360.

[10]Launder, B. E. and Sharma, B. I., "Application of the Energy-Dissipation Model of Turbulence to the Calculation of Flow Near a Spinning Disk," *Letters in Heat and Mass Transfer,* Vol. 1, 1974, pp. 131-138.

[11]Hanjalic, K. and Launder, B. E., "Sensitizing the Dissipation Equation to Irrotational Strains," *Transactions of ASME, Journal of Fluids Engineering,* Vol. 102, 1980, pp. 456-461.

[12]Smith, R. E., "Two-Boundary Grid Generation for the Solution of the Three-Dimensional Compressible Navier-Stokes Equations," NASA TM-83123, 1981.

[13]Yang, S. L. and Shih, T. I-P., "An Algebraic Grid Generation Technique for Time-Varying Two-Dimensional Spatial Domains," *International Journal for Numerical Methods in Fluids,* Vol. 6, 1986, pp. 291-304.

[14]Beam, R. M. and Warming, R. F., "An Implicit Factored Scheme for the Compressible Navier-Stokes Equations," *AIAA Journal,* Vol. 16, 1978, pp. 393-402.

[15]Shih, T. I-P., Smith, G. E., Springer, G. S., and Rimon, Y., "Boundary Conditions for the Solution of the Compressible Navier-Stokes Equations by an Implicit Factored Method," *Journal of Computational Physics,* Vol. 52, 1983, pp. 54-79.